$Ag_{10}Te_4Br_{3-x}Cl_x$ and $Ag_{10}Te_4Br_{3-y}I_y$: Structural and Electrical Property Tuning of a Mixed Conductor by Partial Anion Substitution

Tom Nilges, Melanie Bawohl, and Stefan Lange

Institut für Anorganische und Analytische Chemie, Universität Münster, Corrensstraße 30, 48149 Münster, Germany

Reprint requests to Dr. Tom Nilges. Fax: +49-251-83-36002. E-mail: nilges@uni-muenster.de

Z. Naturforsch. **2007**, *62b,* 955 – 964; received April 5, 2007

Dedicated to Dr. Bernard Chevalier on the occasion of his 60th birthday

X-ray powder and EDX phase analyses, thermal analyses, impedance spectroscopic measurements, and crystal structure determinations of selected phases are reported to highlight the structural and electric properties of the solid solutions $Ag_{10}Te_4Br_{3-x}Cl_x$ and $Ag_{10}Te_4Br_{3-y}I_y$. Bromide can be partially substituted by chloride or iodide up to $x = 1.6$ and $y = 0.2$, respectively, without changes in the structural properties of the tetramorphic, ion-conducting $Ag_{10}Te_4Br_3$. Results from X-ray powder phase analyses have been complemented by data of single crystal structure determinations of selected samples. At r. t. the fully ordered γ-$Ag_{10}Te_4Br_3$ structure type is realized in all chloride containing phases, but a partial iodide substitution leads to the stabilization of the disordered β-$Ag_{10}Te_4Br_3$ structure type. Impedance spectroscopic measurements reveal a significant increase by one order of magnitude of the r. t. silver ion conductivity of $Ag_{10}Te_4Br_{2.8}I_{0.2}$ as compared with $Ag_{10}Te_4Br_3$.

Key words: Silver Ion Conductors, Coinage Metal Polytelluride Halides, Chemical Property Tuning

Introduction

Ion conductors play a crucial role in today's consumer electronics and data storage media. Especially silver ion conductors are drawn back into the focus of materials scientists due to their possible use in non-volatile data storage devices. The extraordinarily high silver ion mobility and the associated fast reaction time for the formation of nano-sized metal spots in suitable media are one of the most favorable properties of these materials [1]. New developments of either materials and/or devices are necessary to satisfy the continuously increasing demand of capacity and storage speed in this field.

Recently we started a systematic exploration of the ternary systems silver-tellurium-halogen in order to prepare new ion-conducting compounds. On the quasibinary section Ag_2Q (Q = chalcogenide except oxygen)-AgX (X = halide) two different classes of compounds with the general formulae Ag_5Q_2X and Ag_3QX are known to date. Starting from Ag_5Te_2Cl [2 – 4] a certain part of either the chalkogenide [5, 6] or the halide substructure [6, 7] can be substituted by lighter or heavier elements of the same group. This substitution takes place with retention of the structural properties but influences the electrical properties of these compounds drastically. Compounds of the type Ag_3SX (X = Cl, Br, I) [8 – 10] were optimized by variation of the halide substructure concerning their total conductivities [11, 12].

Last year we reported on the structural and physical properties of $Ag_{10}Te_4Br_3$ being the first representative of a formerly unseen class of ion conductors [13]. $Ag_{10}Te_4Br_3$ is the first compound containing any of the coinage metals M to enter the phase field M_2Q-MX-Q. Four polymorphs have been characterized in the temperature range from 3 to 340 K [14]. Characteristic features from a topological point of view are 6^3-telluride and 3.6.3.6-bromide nets (Kagomé-like). Covalently bonded polytelluride units (Te_4 units, formed by a Te_2 dumbbell and two additional telluride ions) are additional structural features, characteristic for this mixed conductor.

Silver(I) chalcogenide halides like the aforementioned Ag_3SX^- (X = I, Br, Cl) or Ag_5Q_2X-type (Q = S, Se, Te; X = Cl, Br) can be modified within their anion substructures by a partial substitution of the chalcogenide, as well as the halide part. With retention of the structural properties of the different polymorphs, the phase transition temperatures are adjustable over

a wide range. The high-temperature phases, characterized by high ion conductivities, can be stabilized at temperatures around and below r. t. under certain circumstances. After the discovery of $Ag_{10}Te_4Br_3$ the question arose whether the aforementioned findings can be transferred to the new class of silver(I) polychalcogenide halides.

Results and Discussion

Extensive preparative work was performed to check the possibility of a halide substitution in $Ag_{10}Te_4Br_3$. Within the halide part of the anion substructure it is possible to realize solid solutions by a partial substitution of bromide by chloride or iodide. In order to verify the influence of this partial substitution on the physical and structural properties in $Ag_{10}Te_4Br_3$, we have studied the solid solutions $Ag_{10}Te_4Br_{3-x}Cl_x$ and $Ag_{10}Te_4Br_{3-y}I_y$ by thermal analysis (DSC), X-ray powder diffraction phase analysis, single crystal X-ray structure determinations, and impedance spectroscopy.

Thermal analyses

DSC measurements of selected compounds were performed for the different solid solutions (Fig. 1, Table 1). For $Ag_{10}Te_4Br_{3-x}Cl_x$ the $\delta-\gamma$ and the $\beta-\alpha$ phase transitions are slightly shifted to higher temperatures while the order-disorder transition $\gamma-\beta$ is not affected by an increased chloride content. Starting with a substitution degree of $x = 0.8$ the $\delta-\gamma$ transition can not be detected any more in the DSC thermogram. Structural features of the different polymorphs are given in the following sections.

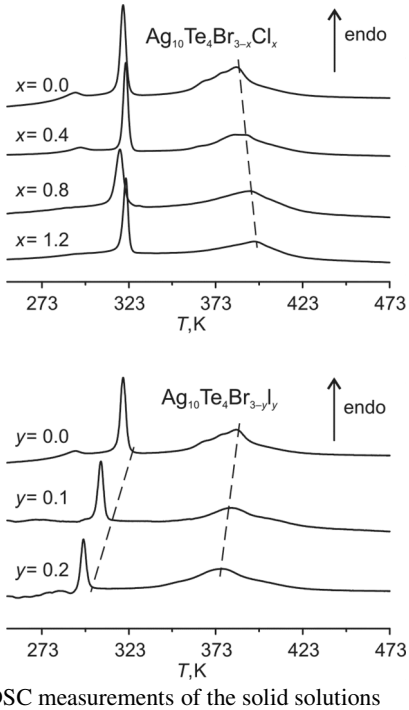

Fig. 1. DSC measurements of the solid solutions $Ag_{10}Te_4Br_{3-x}Cl_x$ and $Ag_{10}Te_4Br_{3-y}I_y$. Dashed lines are added to the figure in order to emphasise the shifts in the phase transition temperatures for the different substitution degrees.

Table 1. Results of DSC measurements (all values in K) for the solid solutions $Ag_{10}Te_4Br_{3-x}Cl_x$ and $Ag_{10}Te_4Br_{3-y}I_y$. The investigated temperature range was 113 to 473 K. Standard deviations in units of the last significant figure are given in parentheses.

	$\delta-\gamma$ (peak maximum)	$\gamma-\beta$ (onset value)	$\beta-\alpha$ (peak maximum)
x ($Ag_{10}Te_4Br_{3-x}Cl_x$)			
0	290(2)	317(1)	385(2)
0.4	295(2)	315(1)	387(2)
0.8	–	309(1)	393(2)
1.2	–	314(1)	396(2)
y ($Ag_{10}Te_4Br_{3-y}I_y$)			
0	290(2)	317(1)	385(2)
0.1	–	300(1)	382(2)
0.2	–	290(1)	376(2)

A partial substitution of bromide in $Ag_{10}Te_4Br_3$ by iodide led to a completely different trend. Even with a substitution degree of $y = 0.1$ the $\delta-\gamma$ transition cannot be observed any more in the investigated temperature range down to 113 K. With an increasing iodide content the $\gamma-\beta$ and $\beta-\alpha$ transitions are shifted towards lower temperatures. This finding can be directly correlated with the differences in size and polarizability of the halides. Starting with a low polarizability and a small size of the chloride in relation to the bromide ions, a lower tendency of the silver ions to interpenetrate the halide nets in the result of Br/Cl substitution. In contrast, only a very small amount of highly polarizable and large iodide is enough to significantly increase the permeability of the halide nets. As a result, the temperature for the order-disorder β-phase transition is reduced drastically by this partial substitution.

X-Ray powder phase analyses

Phase analyses of the solid solutions $Ag_{10}Te_4Br_{3-x}Cl_x$ and $Ag_{10}Te_4Br_{3-y}I_y$ were performed in order to examine the maximum obtainable degrees of substitution and to identify the r. t. polymorphs realized in the process. Phase purity of the samples was achieved up to the maximum substitution

	a (Å)	*b* (Å)	*c* (Å)	*V* (Å^3)	structure type
x ($Ag_{10}Te_4Br_{3-x}Cl_x$)					
0.2	15.377(10)	15.658(8)	13.722(10)	3304(4)	γ-$Ag_{10}Te_4Br_3$
0.4	15.298(7)	15.786(6)	13.601(7)	3284(2)	γ-$Ag_{10}Te_4Br_3$
0.6	15.322(10)	15.466(10)	13.783(13)	3266(5)	γ-$Ag_{10}Te_4Br_3$
0.8	15.326(11)	15.474(18)	13.799(10)	3273(3)	γ-$Ag_{10}Te_4Br_3$
1.0	15.240(9)	15.550(15)	13.695(10)	3246(5)	γ-$Ag_{10}Te_4Br_3$
1.2	15.303(15)	15.448(6)	13.710(7)	3241(5)	γ-$Ag_{10}Te_4Br_3$
1.4	15.310(9)	15.561(13)	13.624(9)	3246(3)	γ-$Ag_{10}Te_4Br_3$
1.6	15.183(9)	15.310(10)	13.747(9)	3196(5)	γ-$Ag_{10}Te_4Br_3$ and β-Ag_5Te_2Cl
1.75					β-Ag_5Te_2Cl and binary phases
y ($Ag_{10}Te_4Br_{3-y}I_y$)					
0.1	13.730(5)		15.352(6)	2506.2(17)	β-$Ag_{10}Te_4Br_3$
0.2	13.767(6)		15.359(5)	2521.0(19)	β-$Ag_{10}Te_4Br_3$
0.3	–[a]		–[a]		β-$Ag_{10}Te_4Br_3$ and additional phases

Table 2. Results of X-ray powder diffraction experiments at 298(1) K for the solid solutions $Ag_{10}Te_4Br_{3-x}Cl_x$ and $Ag_{10}Te_4Br_{3-y}I_y$. Standard deviations of the lattice parameters after least-squares refinements are given in parentheses. Samples of the γ-$Ag_{10}Te_4Br_3$ structure type crystallize in the orthorhombic space group *Cmcm*, and samples of the β-$Ag_{10}Te_4Br_3$-type in the hexagonal space group $P6_3/mmc$ [14]. Data of β-Ag_5Te_2Cl in ref. [4].

[a] Determination of reliable lattice parameters was not possible.

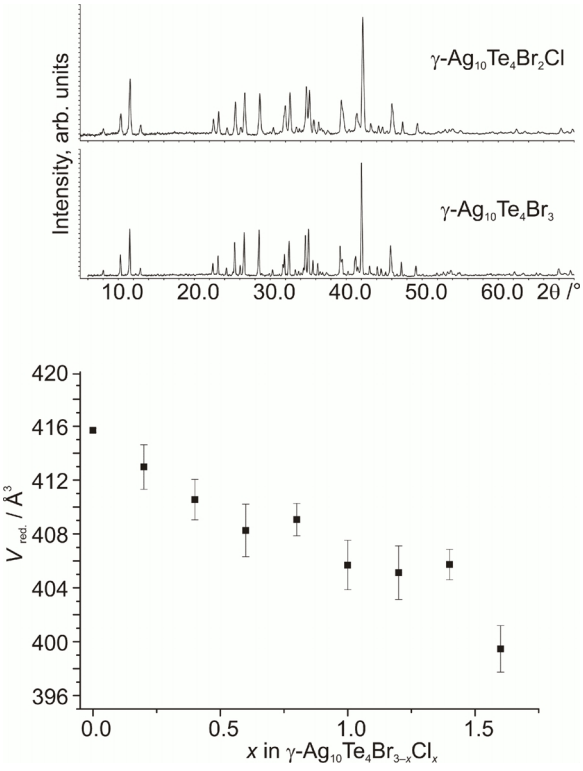

Fig. 2. Top section: X-Ray powder diffractograms of γ-$Ag_{10}Te_4Br_2Cl$ and γ-$Ag_{10}Te_4Br_3$. A significant peak broadening is observed for all quaternary phases. Bottom section: A continuous decrease of the cell volume per formula unit ($V_{red.}$) is found with an increasing degree of substitution *x* in $Ag_{10}Te_4Br_{3-x}Cl_x$. The error bars in the bottom diagram represent a standard deviation of 3σ.

degrees mentioned in the text for both solid solutions. At 298 K the γ-$Ag_{10}Te_4Br_3$ structure type is present in $Ag_{10}Te_4Br_{3-x}Cl_x$ in good accordance with the results from thermal analyses. A continuous decrease of the cell volume was found over the whole *x* range up to $x = 1.6$. γ-$Ag_{10}Te_4Br_{1.4}Cl_{1.6}$ represents the limit for realizable quaternary compounds in this system. Small deviations from a Vegard-like behaviour have been observed for the compositions $x = 0.8$ and 1.4 and are probably due to the low overall crystallinity of the samples, drastically affecting the precision of the determination of the lattice parameters. A significant peak broadening is observed for all quaternary compounds compared with γ-$Ag_{10}Te_4Br_3$, as shown in Fig. 2. At a higher degree of substitution than $x = 1.6$ a formation of quaternary compounds was not observed any more and β-Ag_5Te_2Cl [4] and binary phases resulted.

In the system $Ag_{10}Te_4Br_{3-y}I_y$ the maximum degree of substitution is $y = 0.2$ (Table 2).

This value is much lower than the respective one for $Ag_{10}Te_4Br_{3-x}Cl_x$. Nevertheless the detected phase transition around r. t., from the ordered γ-$Ag_{10}Te_4Br_3$-type to the disordered β-$Ag_{10}Te_4Br_3$-type, has also been substantiated by the phase analyses.

Even for a value of $y = 0.1$ with a $\gamma - \beta$ phase transition temperature of 300(1) K the β-type was detected by X-ray phase analysis. Table 2 summarizes the lattice parameters for the different representatives of the solid solutions.

Focussing on the ion conductivity performance the stabilization of the highly disordered β-phase at r. t. is the key finding of this halide substitution study. A significant change in the electrical properties can be expected for the substituted phases. In order to support the aforementioned results, single crystal structure determinations of selected compounds and a determina-

tion of the partial ionic conductivity of the maximally substituted iodide phase were performed.

Single crystal X-ray structure determinations

In order to substantiate the results from X-ray powder phase analyses, single crystals of representative solid solutions were selected for r. t. X-ray structure determinations. Suitable single crystals were isolated from the bulk phases with the nominal compositions $Ag_{10}Te_4Br_2Cl$ and $Ag_{10}Te_4Br_{2.8}I_{0.2}$. The lattice parameters and cell volumes derived from the IPDS II diffractometer data (see Table 3) were compared with the lattice parameters derived from phase analyses, always keeping the systematic errors for both methods in mind. The composition of the chloride-containing crystal appeared to be close to $Ag_{10}Te_4Br_{2.6}Cl_{0.4}$ while the iodide-containing crystal showed an excellent match for the maximally substituted phase $Ag_{10}Te_4Br_{2.8}I_{0.2}$. A small deviation of composition from one crystal to another of the same reaction batch was found by EDX analyses. Examples for different batches are given in Table 9 in the Experimental Section. This finding is typical for solid solutions and can only be avoided by time-consuming homogenization and annealing processes.

After correction for Lorentz polarization and absorption effects a structure refinement was carried out on the basis of the γ- and β-$Ag_{10}Te_4Br_3$ structure types [14]. Following the general refinement procedure for compounds with highly disordered ions, a non-harmonic approach [15 – 18] for the distribution of the silver ions was applied to some silver positions. This approach is well suited for materials characterized by disorder phenomena and is regularly used for the description of the ion distribution in ion conductors [4 – 6, 19]. Atomic coordinates of the non-harmonically refined positions, often called mode positions, are marked with a suffix *m*, representing the maximum of probability density. In the final refinement stages the site occupancy factors of all halide positions were refined with mixed halide occupancy, restricted only to an overall full occupancy for each position. A selection of crystallographic data is summarized in Table 3. Atomic coordinates, site occupancy factors and displacement parameters are given in Tables 4 – 6.

The refined compositions of $Ag_{10}Te_4Br_{2.4(2)}Cl_{0.6(2)}$ and $Ag_{10}Te_4Br_{2.7(1)}I_{0.3(1)}$ are close to the estimated compositions of $Ag_{10}Te_4Br_{2.6}Cl_{0.4}$ and $Ag_{10}Te_4Br_{2.8}I_{0.2}$ derived from phase-analytical experiments.

Table 3. Selected crystallographic data of $Ag_{10}Te_4Br_{2.4(2)}Cl_{0.6(2)}$ and $Ag_{10}Te_4Br_{2.7(1)}I_{0.3(1)}$.

Composition	$Ag_{10}Te_4Br_{2.4(2)}Cl_{0.6(2)}$	$Ag_{10}Te_4Br_{2.7(1)}I_{0.3(1)}$
Structure type	γ-$Ag_{10}Te_4Br_3$	β-$Ag_{10}Te_4Br_3$
M_r, g mol^{-1}	1802.3	1844.9
Crystal size, mm^3	$0.03 \times 0.02 \times 0.02$	$0.06 \times 0.05 \times 0.05$
Color	dark grey	
Crystal system	orthorhombic	hexagonal
Space group	*Cmcm* (No. 63)	$P6_3/mmc$ (No. 194)
Lattice parameters		
a, Å	15.347(3)	13.759(2)
b, Å	15.659(2)	*a*
c, Å	13.691(2)	15.356(2)
V_{EZ}, Å^3	3290.2(9)	2517.6(6)
Z	8	6
D_{calcd}, g cm^{-3}	7.28	7.30
Diffractometer	Stoe IPDS II	
	MoK_α radiation (λ = 0.71073 Å), graphite monochromator	
ω Range, deg	0.0 – 180.0	0.0 – 180.0
$\Delta\omega$, deg	1.0	1.0
μ (MoK_α), mm^{-1}	24.5	25.1
Absorp. correction	numerical, X-RED and X-SHAPE [23]	
Temperature, K	293	
θ Range	1.86 – 25.70	2.16 – 30.56
hkl Range	$-18 \le h \le 18$	$-19 \le h \le 18$
	$-16 \le k \le 19$	$-16 \le k \le 19$
	$-16 \le l \le 14$	$-21 \le l \le 21$
Refl. measured	9093	16157
Refl. unique	1687	1480
R_{int}	0.1387	0.1894
Refinement	least-squares on F^2; Gram-Charlier non-harmonic expansion	
Program	JANA2000 [24]	
R [$I \ge 3\sigma$ (I)]	0.0546	0.0223
wR [$I \ge 3\sigma$ (I)]	0.0621	0.0240
R (all)	0.1868	0.1181
wR (all)	0.0782	0.0369
Param. refined	120	191
Gof (F^2)	1.54	1.81
Max/min. resid. electron density, e Å^{-3}	3.58/−3.50	1.92/−2.17

A detailed description of the structural features can be found in references [13, 14] and only a brief summary is given in the caption of Fig. 3, where a schematic overview of the four known polymorphs of the $Ag_{10}Te_4Br_3$-type is given.

In the ordered γ-phase silver is distributed around the tellurium substructure and the halide substructure acts as a separator for the silver ions, leading to a predominantly 2-dimensional silver mobility along the 6^3 Te nets. Silver is also located in direct neighbourhood to the Te_4 units in an almost linear coordination to form $^1_\infty[Te_4Ag]$ strands. Within

Table 4. Atomic coordinates, site occupancy factors (sof), and isotropic displacement parameters (Å^2) of $Ag_{10}Te_4Br_{2.4(2)}Cl_{0.6(2)}$ at 293 K with estimated standard deviations in parentheses. Mode positions (suffix m) were derived from the single probability density function (pdf) of the respective position. They represent the maximum of probability to find an atom in a certain volume element.

Atom	Wyckoff	sof	x	y	z	U_{iso}
Te1	8*g*	1	0.17507(13)	0.1257(3)	1/4	0.0181(9)
Te2	8*g*	1	0.09140(16)	0.6183(3)	1/4	0.0330(10)
Te3	8*f*	1	0	−0.1204(3)	0.0883(2)	0.0322(10)
Te4	8*f*	1	0	0.3754(3)	0.0535(2)	0.0332(10)
Br1	8*e*	0.79(4)	0.2498(4)	1/2	0	0.037(3)
Cl1	8*e*	0.21	0.2498(4)	1/2	0	0.037(3)
Br2	8*d*	0.86(5)	1/4	3/4	1/2	0.061(4)
Cl2	8*d*	0.14	1/4	3/4	1/2	0.061(4)
Br3	8*g*	0.74(2)	0.2422(3)	0.8712(6)	1/4	0.0347(19)
Cl3	8*g*	0.26	0.2422(3)	0.8712(6)	1/4	0.0347(19)
Ag1	4*c*	1	0	0.1483(5)	1/4	0.078(3)
Ag2	4*c*	1	0	0.3948(10)	1/4	0.091(5)
Ag3	16*h*	1	0.1243(5)	0.4789(6)	0.1347(5)	0.114(2)
Ag4	16*h*	1	0.1156(3)	0.2618(4)	0.1358(4)	0.0947(19)
Ag5	8*g*	1	0.0956(4)	−0.0300(4)	1/4	0.125(4)
Ag6	16*h*	1	0.1016(3)	0.0818(4)	0.0692(3)	0.139(2)
Ag7	16*h*	1	0.1166(4)	0.7250(8)	0.3908(9)	0.302(6)
Ag3m	*mode pos.*		0.1344	0.4727	0.1329	
Ag4m	*mode pos.*		0.1112	0.2627	0.1392	
Ag5m	*mode pos.*		0.089	−0.0333	1/4	
Ag7m	*mode pos.*		0.1165	0.7489	0.38	

Table 5. Atomic coordinates, site occupancy factors (sof), and isotropic displacement parameters (Å^2) of $Ag_{10}Te_4Br_{2.7(1)}I_{0.3(1)}$ at 293 K. Estimated standard deviations are given in parentheses. Mode positions (suffix m) were derived from the single probability density function (pdf) of the respective position. They represent the maximum of probability to find an atom in a certain volume element.

Atom	Wyckoff	sof	x	y	z	U_{iso}
Te1	4*f*	1	2/3	1/3	0.42144(17)	0.0309(11)
Te2	4*f*	1	2/3	1/3	0.6589(2)	0.0357(11)
Te3	12*j*	1	0.3447(3)	0.00958(17)	3/4	0.0443(12)
Te4a	4*e*	0.45(3)	0	0	0.6525(14)	0.053(6)
Te4b	4*e*	0.54	0	0	0.5912(9)	0.022(3)
Br1	6*g*	0.92(4)	1/2	0	1/2	0.044(3)
I1	6*g*	0.08	1/2	0	1/2	0.044(3)
Br2	12*k*	0.86(2)	0.1668(2)	2*x*	−0.0028(2)	0.0452(15)
I2	12*k*	0.14	0.1668(2)	2*x*	−0.0028(2)	0.0452(15)
Ag1	2*d*	0.76(2)	2/3	1/3	1/4	0.044(3)
Ag1b	12*i*	0.19(1)	0.110(2)	0	1/2	0.119(13)
Ag2	12*k*	0.44(3)	0.0950(10)	2*x*	0.213(3)	0.34(2)
Ag2b	12*k*	0.41(2)	0.1236(11)	2*x*	0.7187(14)	0.153(8)
Ag3	24*l*	0.49(2)	0.316(2)	−0.1568(13)	0.6436(8)	0.137(12)
Ag4	24*l*	0.44(2)	0.4853(16)	0.1319(12)	0.6217(9)	0.128(6)
Ag5	12*k*	0.23(2)	0.244(2)	2*x*	0.702(3)	0.31(3)
Ag6	12*k*	0.37(3)	0.4480(10)	2*x*	0.6605(15)	0.093(10)
Ag7	12*k*	0.37(3)	0.2224(17)	2*x*	0.154(2)	0.23(3)
Ag8	24*l*	0.34(1)	0.005(2)	0.191(2)	0.6272(15)	0.138(11)
Ag9	24*l*	0.164(8)	−0.017(4)	0.296(4)	0.5868(14)	0.20(3)
Ag1bm	*mode pos.*		0.1051	0	1/2	
Ag2m	*mode pos.*		0.1101	2*x*	0.1946	
Ag2bm	*mode pos.*		0.1138	−0.1138	0.7155	
Ag3m	*mode pos.*		0.3171	−0.161	0.6396	
Ag4m	*mode pos.*		0.4778	0.129	0.6149	
Ag6m	*mode pos.*		0.4434	2*x*	0.6677	
Ag7m	*mode pos.*		0.4454	0.2227	0.6472	
Ag8m	*mode pos.*		−0.0077	0.1986	0.6204	
Ag9m	*mode pos.*		0	0.3144	0.5916	

the two high-temperature polymorphs the situation changes and a partial 3-dimensional distribution and interpenetration of silver through the Kagomé Br nets occurs. In addition a structural frustration of the aforementioned Te_4 units results due to the loss of the linearly coordinating silver along the $^1_\infty[Te_4Ag]$ strands.

The substitution within the halide substructure leads to a retention of the structural features of the ternary phases. In good accordance with the results from ther-

Table 6. Anisotropic displacement parameters (Å^2) for $Ag_{10}Te_4Br_{2.4(2)}Cl_{0.6(2)}$ and $Ag_{10}Te_4Br_{2.7(1)}I_{0.3(1)}$ at 293 K.

Atom	U_{11}	U_{22}	U_{33}	U_{12}	U_{13}	U_{23}
$Ag_{10}Te_4Br_{2.4(2)}Cl_{0.6(2)}$						
Te1	0.0134(12)	0.0250(17)	0.0158(16)	0.0010(17)	0	0
Te2	0.0191(14)	0.0229(19)	0.057(2)	0.0031(18)	0	0
Te3	0.0371(15)	0.041(2)	0.0186(17)	0	0	0.001(2)
Te4	0.0277(15)	0.039(2)	0.0329(19)	0	0	0.007(3)
Br1	0.034(5)	0.058(6)	0.020(5)	0	0	0.004(5)
Cl1	0.034(5)	0.058(6)	0.020(5)	0	0	0.004(5)
Br2	0.033(5)	0.091(8)	0.060(8)	−0.003(4)	0.018(3)	−0.016(6)
Cl2	0.033(5)	0.091(8)	0.060(8)	−0.003(4)	0.018(3)	−0.016(6)
Br3	0.026(3)	0.026(3)	0.052(4)	0.000(3)	0	0
Cl3	0.026(3)	0.026(3)	0.052(4)	0.000(3)	0	0
Ag3	0.116(4)	0.137(5)	0.089(3)	−0.090(4)	0.051(3)	−0.048(4)
Ag4	0.108(3)	0.100(4)	0.076(3)	0.069(3)	0.045(3)	0.057(3)
Ag5	0.052(3)	0.040(3)	0.283(11)	−0.002(3)	0	0
Ag6	0.125(3)	0.220(6)	0.073(3)	0.110(4)	−0.063(3)	−0.089(4)
Ag7	0.092(4)	0.548(16)	0.266(9)	0.069(6)	−0.057(5)	−0.311(10)
Ag1	0.010(3)	0.086(7)	0.138(7)	0	0	0
Ag2	0.035(3)	0.195(13)	0.043(4)	0	0	0
$Ag_{10}Te_4Br_{2.7(2)}I_{0.3(2)}$						
Te1	0.0366(14)	0.0366(14)	0.0196(17)	0.0183(7)	0	0
Te2	0.0451(14)	0.0451(14)	0.0169(17)	0.0226(7)	0	0
Te3	0.0494(16)	0.0384(16)	0.0545(8)	0.0291(12)	0	0
Te4a	0.061(6)	0.061(6)	0.039(12)	0.031(3)	0	0
Te4b	0.021(3)	0.021(3)	0.023(8)	0.0104(14)	0	0
Br1	0.056(4)	0.034(4)	0.036(3)	0.0171(19)	0.0033(17)	0.007(3)
I1	0.056(4)	0.034(4)	0.036(3)	0.0171(19)	0.0033(17)	0.007(3)
Br2	0.044(2)	0.0445(18)	0.047(2)	0.0221(11)	0.004(3)	0.0020(17)
I2	0.044(2)	0.0445(18)	0.047(2)	0.0221(11)	0.004(3)	0.0020(17)
Ag1	0.065(5)	0.065(5)	0.003(3)	0.033(2)	0	0
Ag1b	0.080(10)	0.17(2)	0.137(19)	0.085(10)	−0.019(6)	−0.038(12)
Ag2	0.159(13)	0.31(3)	0.60(5)	0.156(14)	0.135(15)	0.27(3)
Ag2b	0.068(6)	0.068(6)	0.239(19)	−0.029(6)	0.049(7)	−0.049(7)
Ag3	0.30(2)	0.115(10)	0.070(5)	0.159(14)	−0.059(8)	−0.049(5)
Ag4	0.165(11)	0.058(6)	0.068(6)	−0.013(5)	0.063(7)	−0.012(4)
Ag5	0.29(3)	0.29(3)	0.37(5)	0.15(3)	0.15(2)	−0.15(2)
Ag6	0.106(19)	0.025(8)	0.122(13)	0.013(4)	−0.013(4)	−0.026(9)
Ag7	0.038(10)	0.37(6)	0.18(2)	0.019(5)	−0.033(12)	−0.016(6)
Ag8	0.169(13)	0.111(14)	0.114(12)	0.056(11)	−0.019(12)	−0.066(11)
Ag9	0.25(4)	0.40(5)	0.037(9)	0.23(4)	0.000(12)	0.010(16)

Table 7. Selected interatomic distances (Å) for $Ag_{10}Te_4Br_{2.4(2)}Cl_{0.6(2)}$ and $Ag_{10}Te_4Br_{2.7(1)}I_{0.3(1)}$ at 293 K calculated with respect to the maxima of probability density (mode position) in case of non-harmonically refined positions derived from the respective singe pdf. The estimated standard deviations are less than 0.007 Å in case of $Ag_{10}Te_4Br_{2.4(2)}Cl_{0.6(2)}$ and less than 0.03 Å for $Ag_{10}Te_4Br_{2.7(1)}I_{0.3(1)}$.

	d (Å)		d (Å)		d (Å)		d (Å)
$Ag_{10}Te_4Br_{2.4(2)}Cl_{0.6(2)}$				Te1–Ag6m	2.959	Te4b–Te4b	2.80
Te1–Ag6	2.806	Te4–Ag2	2.707	Te2–Te2	2.798	Te4b–Ag1bm	2.013
Te1–Ag1	2.710	Te4–Ag3m	2.785	Te2–Ag4m	2.794	Te4b–Ag2m	3.067
Te1–Ag4m	2.804	Te4–Ag4m	2.721	Te2–Ag7m	2.643	Te4b–Ag8m	2.823
Te1–Ag5m	2.819	Br1–Ag6	2.782	Te3–Ag5	3.13	Br1–Ag4m	2.627
Te2–Te2	2.805	Br1–Ag3m	2.575	Te3–Ag2m	2.818	Br1–Ag6m	2.907
Te2–Ag3m	2.864	Br2–Ag4m	2.8652	Te3–Ag2bm	2.804	Br1–Ag9m	2.949
Te2–Ag7m	2.738	Br2–Ag7m	2.6262	Te3–Ag3m	2.763	Br2–Ag1bm	2.817
Te3–Ag6	2.729	Br3–Ag3m	2.947	Te3–Ag4m	2.711	Br2–Ag3m	2.920
Te3–Ag5m	2.937	Br3–Ag5m	2.786	Te3–Ag6m	2.931	Br2–Ag4m	2.917
Te3–Ag7m	2.752			Te3–Ag7m	2.991	Br2–Ag7m	2.661
				Te3–Ag8m	2.746	Br2–Ag8m	2.831
$Ag_{10}Te_4Br_{2.7(1)}I_{0.3(1)}$				Te3–Ag9m	2.470	Br2–Ag8m	2.758
Te1–Ag1	2.633	Te4a–Ag2m	2.702	Te4a–Te4a	2.99	Br2–Ag9m	2.651
Te1–Ag5	2.85	Te4a–Ag2bm	2.879	Te4a–Te4b	0.94	Br2–Ag9m	2.505
Te1–Ag3m	2.661	Te4a–Ag8m	2.830	Te4a–Ag1bm	2.75		

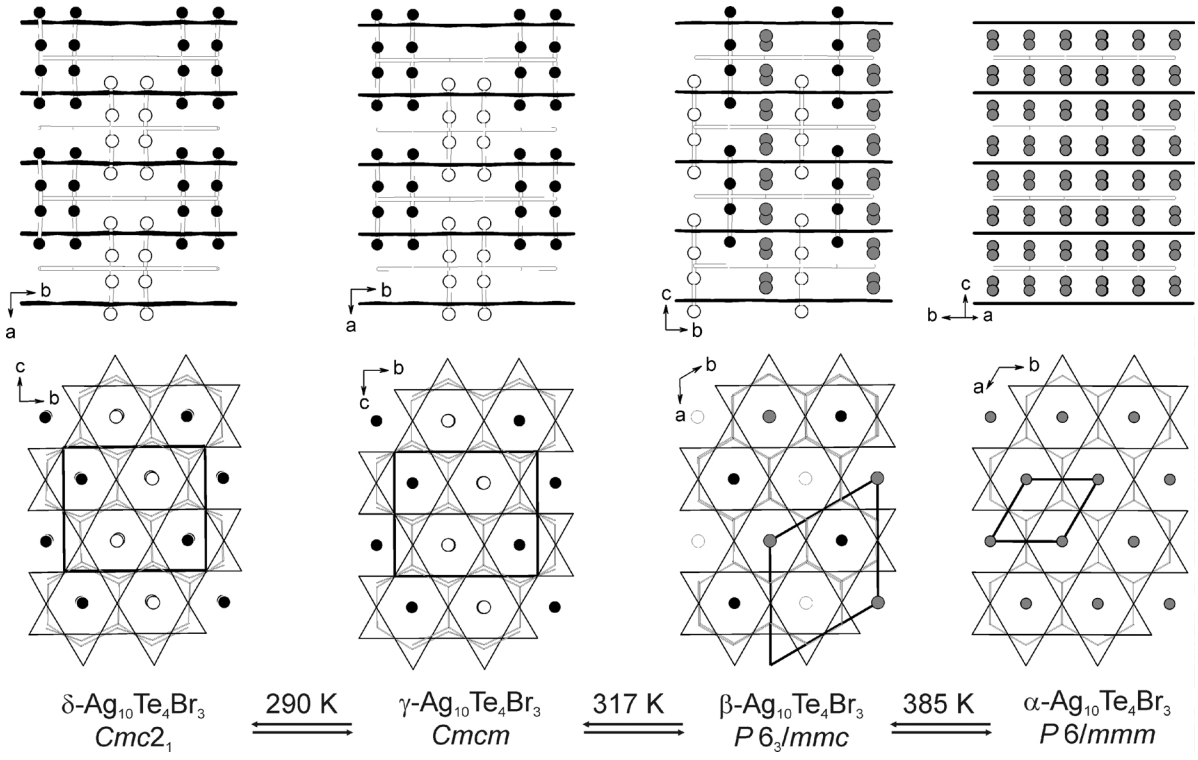

Fig. 3. Schematic representations of the anion substructures of the four $Ag_{10}Te_4Br_3$ structure types according to ref. [14] (385 K represents the peak maximum instead of 355 K, which was derived from the onset value in [14]). Nets of isolated Te^{2-} and Br^- ions with homonuclear distances larger than two times their van der Waals radii are drawn by solid black and grey lines. Two different representations of Te_4 units, formed by a $[Te_2]^{2-}$ dumbbell and two additional tellurium atoms, are drawn as black solid spheres and open spheres with respect to their relative heights in relation to the residual anion substructure. Structurally frustrated Te_4 units resulting in half-occupied Te positions are represented by dark grey spheres.

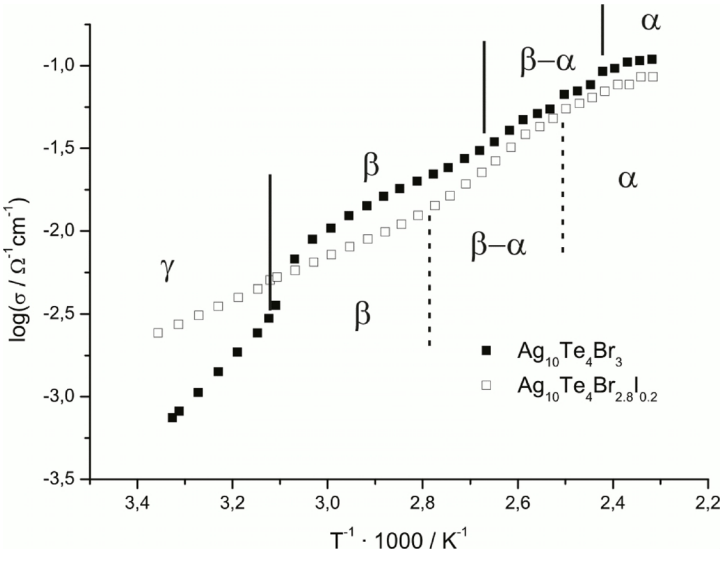

Fig. 4. Arrhenius representation of the ionic conductivity of $Ag_{10}Te_4Br_3$ (data from ref. [14]) and $Ag_{10}Te_4Br_{2.8}I_{0.2}$. Changes in the partial ionic conductivity in both cases are directly correlated with the phase transitions observed in thermal analyses and structure determinations. Solid black lines ($Ag_{10}Te_4Br_3$) and dashed grey lines ($Ag_{10}Te_4Br_{2.8}I_{0.2}$) represent the regions of phase transitions for both compounds. An increase of approximately one order of magnitude is present after the partial substitution of bromide by chloride around r. t. ($\log\sigma = -3.36$ is equivalent to 298 K).

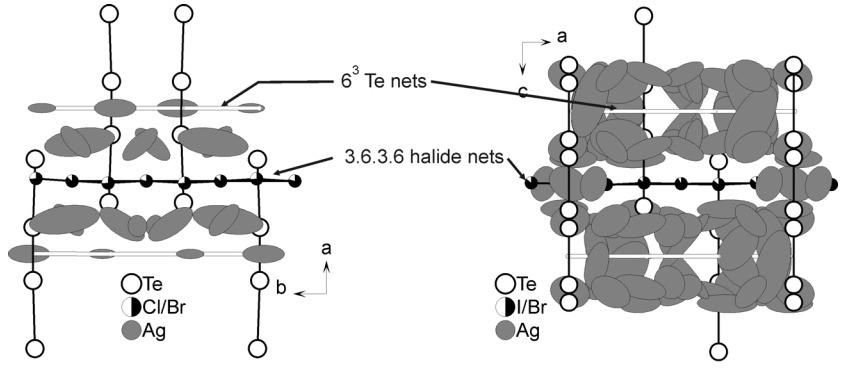

γ-$Ag_{10}Te_4Br_{2.4(2)}Cl_{0.6(2)}$ β-$Ag_{10}Te_4Br_{2.7(1)}I_{0.3(1)}$

Fig. 5. Sections of the crystal structure of the γ- and β-$Ag_{10}Te_4Br_3$ structure type for γ-$Ag_{10}Te_4Br_{2.4(2)}Cl_{0.6(2)}$ and β-$Ag_{10}Te_4Br_{2.8(1)}I_{0.2(1)}$ representing the region around the Kagomé-like 3.6.3.6 halide nets. The 2-dimensional silver distribution around the telluride substructure for the γ-type is accompanied by a partial 3-dimensional distribution for the β-$Ag_{10}Te_4Br_3$ structure type. Silver is interpenetrating the Kagomé nets in the β-phase. White sectors within the black halide spheres represent the amounts of chloride or iodide on these positions. Silver displacement parameters are drawn at the 90 % probability level.

Table 8. Partial specific ion conductivities of $Ag_{10}Te_4Br_3$ (data from ref. [14]) and $Ag_{10}Te_4Br_{2.8}I_{0.2}$.

$Ag_{10}Te_4Br_3$		$Ag_{10}Te_4Br_{2.8}I_{0.2}$	
T, K	$\sigma(\Omega^{-1}\,cm^{-1})$	T, K	$\sigma(\Omega^{-1}\,cm^{-1})$
301	7.5×10^{-4}	298	2.4×10^{-3}
302	8.2×10^{-4}	302	2.7×10^{-3}
306	1.1×10^{-3}	306	3.1×10^{-3}
310	1.4×10^{-3}	310	3.5×10^{-3}
314	1.9×10^{-3}	314	4.0×10^{-3}
318	2.4×10^{-3}	318	4.5×10^{-3}
320	3.0×10^{-3}	320	5.1×10^{-3}
322	3.6×10^{-3}	322	5.3×10^{-3}
326	6.8×10^{-3}	326	5.8×10^{-3}
330	8.9×10^{-3}	330	6.5×10^{-3}
334	1.0×10^{-2}	334	7.2×10^{-3}
338	1.2×10^{-2}	339	8.0×10^{-3}
343	1.4×10^{-2}	343	9.0×10^{-3}
347	1.6×10^{-2}	347	9.9×10^{-3}
351	1.8×10^{-2}	352	1.1×10^{-2}
356	2.0×10^{-2}	356	1.2×10^{-2}
360	2.2×10^{-2}	360	1.4×10^{-2}
364	2.4×10^{-2}	365	1.6×10^{-2}
369	2.8×10^{-2}	369	1.9×10^{-2}
373	3.1×10^{-2}	374	2.3×10^{-2}
377	3.5×10^{-2}	378	2.7×10^{-2}
382	4.1×10^{-2}	383	3.2×10^{-2}
386	4.7×10^{-2}	387	3.9×10^{-2}
391	5.1×10^{-2}	392	4.3×10^{-2}
395	5.5×10^{-2}	396	4.8×10^{-2}
400	6.7×10^{-2}	400	5.5×10^{-2}
404	7.0×10^{-2}	405	5.9×10^{-2}
409	7.7×10^{-2}	409	6.4×10^{-2}
413	9.3×10^{-2}	414	7.0×10^{-2}
417	9.7×10^{-2}	418	7.7×10^{-2}
422	1.1×10^{-1}	423	7.7×10^{-2}
427	1.1×10^{-1}	427	8.6×10^{-2}
431	1.1×10^{-1}	432	8.6×10^{-2}

mal analyses the γ-$Ag_{10}Te_4Br_3$ structure type is realized for $Ag_{10}Te_4Br_{2.4}Cl_{0.6}$, and the β-$Ag_{10}Te_4Br_3$-type for the iodide-containing phase at 298 K. A statistical distribution of the halide ions on the halide positions was observed in both cases (Tables 4 and 5). All bond lengths are within the expected regions for Ag–Te, Ag–X (X = halide) and Te–Te bonds (Table 7).

Impedance spectroscopy

Impedance measurements of $Ag_{10}Te_4Br_{2.8}I_{0.2}$ were performed in order to investigate the influence of the substitution on the partial ionic conductivity (Table 8).

For $Ag_{10}Te_4Br_{2.8}I_{0.2}$ the silver ion conductivity shows an Arrhenius-type behaviour with a linear increase of conductivity with temperature in the regions of existence of the β-$Ag_{10}Te_4Br_3$- as well as the α-$Ag_{10}Te_4Br_3$-type (Fig. 4).

A more drastic increase of conductivity takes place in the broad temperature range of the $\beta-\alpha$ phase transition where the exclusively 2-dimensional mobility along the telluride nets changes to a partially 3-dimensional mobility with a contribution of silver transport through the halide nets (see Fig. 5). This finding is in accordance with the observation for $Ag_{10}Te_4Br_3$. Especially in the interesting region around r. t. an increase of about one order of magnitude can be observed as compared to the non-substituted ternary phase.

The activation energies are not significantly affected by the substitution as can be seen from the slopes of the respective impedance plots in Fig. 4.

Conclusion

The halide substructure of tetramorphic $Ag_{10}Te_4Br_3$ can be partially substituted by chloride or iodide ions up to maximum substitution degrees of $x = 1.6$ for $Ag_{10}Te_4Br_{3-x}Cl_x$ and $y = 0.2$ for $Ag_{10}Te_4Br_{3-y}I_y$. At higher chloride contents and after an iodide substitution the low temperature $\delta - \gamma$ phase transition can be completely suppressed while the two high-temperature transitions $\gamma - \beta$ and $\beta - \alpha$, are shifted over a certain temperature region. An opposite trend of these shifts can be induced by the different halide substitutions. Chloride ions increase the high-temperature $\beta - \alpha$ transition while iodide ions decrease both the $\gamma - \beta$ and $\beta - \alpha$ transition. A stabilization of the β-$Ag_{10}Te_4Br_3$ structure, characterized by a strongly disordered silver substructure, is possible down to r. t. in $Ag_{10}Te_4Br_{2.8}I_{0.2}$. An increase of the ionic conductivity of almost one order of magnitude was observed for $Ag_{10}Te_4Br_{2.8}I_{0.2}$ compared with $Ag_{10}Te_4Br_3$. The chemical modification of the halide substructure is a powerful chemical tool to tune the electrical properties of these materials over a certain temperature range.

Experimental Section

Synthesis

The solid solutions were prepared from mixtures (total mass approx. 1 g) of silver (Chempur, 99.9 %), tellurium (Chempur, 99.999 %), silver(I) chloride (AlfaAesar, 99.9 %), silver(I) bromide (Chempur, 99+ %) and silver(I) iodide (Sigma Aldrich, 99 %) in evacuated ($p < 10^{-3}$ mbar) silica ampoules. A one day heating stage at 1223 K was applied to the bulk samples and the hot ampoules were transferred to an ice bath afterwards. Three to five homogenization and annealing stages (at 613 K and 14 days for $Ag_{10}Te_4Br_{3-x}Cl_x$ and at 623 K and 21 days for $Ag_{10}Te_4Br_{3-y}I_y$) were passed in order to achieve phase purity for all samples.

$RbAg_4I_5$, used for electron blocking electrodes in the impedance spectroscopic measurements, was prepared by mixing AgI (Sigma Aldrich, 99 %) and RbI (AlfaAesar, 99.8 %) in a 4 : 1 molar ratio in evacuated silica ampoules, subsequent heating to 973 K and quenching in an ice bath. The phase-pure $RbAg_4I_5$ was stored at 323 K prior to use and each electrode was prepared immediately before the measurements.

Thermal analyses

DSC measurements were performed using a Netzsch DSC 204t calorimeter under N_2 atmosphere in aluminium crucibles. Hg, In, Sn, Bi, Zn, and CsCl were used for calibration and a temperature accuracy of ±1 K could be estimated from the calibration measurements for onset values. A temperature range of 113 to 473 K was applied to each sample under discussion. The heating rate was 10 K min^{-1} in all cases. At least two consecutive runs were measured for each sample in order to check the reversibility of the observed effects. All results are derived from the second heating run for each sample. A standard deviation of ±2 K was estimated for the derived values at the peak maxima based on the signal broadening at this position.

Impedance spectroscopy

Partial ionic conductivities were measured using a symmetrical setup with two electron-blocking, but silver ion-conducting electrodes ($RbAg_4I_5$) according to the well known electrochemical concepts introduced by C. Wagner [20] and applied by many others since then [14, 21, 22]. Details about the electrode/sample setup are given elsewhere [14]. A cold-pressed pellet of $Ag_{10}Te_4Br_{2.8}I_{0.2}$ was mounted to $RbAg_4I_5$ electrode pellets and contacted *via* pressed silver powder to platinum electrodes to achieve a symmetrical electrode setup. The whole unit was mounted to a homemade measuring cell and was transferred to a Julabo MW4 tempering unit. A Solatron 1260 frequency response analyzer and a Solatron 1287 potentiostat were used to record impedance spectra under N_2 atmosphere in a temperature range between 301 and 433 K. Impedance spectra were recorded in the frequency range of 1 MHz to 0.1 Hz allowing 1 h of equilibration time between each set of measurements to achieve temperature constancy at the sample. After each set of impedance measurements for a certain temperature a dc measurement was carried out by applying a dc potential difference (±10 mV) and taking the steady state ionic current after 400 s. The resulting resistance was also used to calculate the ionic conductivity. Both ionic conductivities derived from the low frequency part of the impedance spectra and the dc steady state current agreed well within the estimated errors of the experiments.

X-Ray powder diffraction

X-Ray powder phase analysis was performed using a Stoe StadiP X-ray powder diffractometer operated with Cu$K_{\alpha 1}$ radiation (λ = 1.54051 Å) and equipped with a linear 5° position-sensitive detector (PSD). Silicon was used as external standard. All measurements were carried out at 298(1) K.

X-Ray single crystal structure analysis

Intensity data were collected on a Stoe IPDS II diffractometer with MoK_α radiation (λ = 0.71073 Å). All data sets were corrected for Lorentz, polarization and absorption effects.

The programs X-RED and X-SHAPE [23] were applied to optimize the crystal shape from symmetry-equivalent re-

flections, in order to perform a numerical absorption correction. All space groups were derived from the systematic extinctions, and superstructure formation was excluded by a careful analysis of precession photographs. The structures were refined [24] using the γ-$Ag_{10}Te_4Br_3$ or β-$Ag_{10}Te_4Br_3$ structure types as models [14] by applying a non-harmonical Gram-Charlier approach for the description of parts of the highly disordered silver substructure.

Further details of the crystal structure determinations can be obtained from the Fachinformationszentrum Karlsruhe, 76344 Eggenstein-Leopoldshafen, Germany (fax: +49-7247-808-666; e-mail: crysdata@fiz-karlsruhe.de; http://www.fiz-informationsdienste.de/en/DB/icsd/depot_anforderung.html) on quoting the deposition numbers CSD-417995 ($Ag_{10}Te_4Br_{2.4}Cl_{0.6}$) and CSD-417996 ($Ag_{10}Te_4Br_{2.7}I_{0.3}$).

EDX Measurements

Semiquantitative analyses of selected samples were carried out using a Leica 420i scanning electron microscope fitted with an energy-dispersive detector (EDX, Oxford). Silver, HgTe, KBr and KCl were used as calibration standards. A voltage of 20 kV was applied to the samples. A summary of the analyses is given in Table 9.

Table 9. Results of EDX measurements (in at %) of selected samples of the solid solutions $Ag_{10}Te_4Br_{3-x}Cl_x$ and $Ag_{10}Te_4Br_{3-y}I_y$.

	Ag	Te	Br	I/Cl
$Ag_{10}Te_4Br_{2.5}I_{0.5}$				
theoretical	*58.8*	*23.5*	*14.7*	*2.9*
sample 1	57(2)	21(2)	18(2)	4(2)
sample 2	57(2)	23(2)	17(2)	3(2)
sample 3	55(2)	24(2)	18(2)	4(2)
average	*56(2)*	*23(2)*	*18(2)*	*4(2)*
$Ag_{10}Te_4Br_{1.5}Cl_{1.5}$				
theoretical	*58.8*	*23.5*	*8.8*	*8.8*
sample 1	61(2)	26(2)	3(2)	9(2)
sample 2	61(2)	25(2)	5(2)	10(2)
sample 3	62(2)	24(2)	3(2)	11(2)
sample 4	57(2)	25(2)	9(2)	9(2)
average	*60(2)*	*25(2)*	*5(2)*	*10(2)*

Acknowledgements

This work was financed by the DFG within the SFB 458 'Ionenbewegung in Materialien mit ungeordneten Strukturen'. The DSC measurements performed by W. Prösting and the access to impedance equipment granted by Prof. Dr. H.-D. Wiemhöfer (both Universität Münster) are gratefully acknowledged.

[1] M. N. Kozicki, M. Mitkova, M. Park, M. Balakrishnan, C. Gopalan, *Superlattices Microstruct*. **2003**, *34*, 459.
[2] R. Blachnik, H. A. Dreisbach, *J. Solid State Chem*. **1985**, *60*, 115.
[3] T. Doert, E. Rönsch, F. Schnieders, P. Böttcher, J. Sieler, *Z. Anorg. Allg. Chem*. **2000**, *626*, 89.
[4] T. Nilges, S. Nilges, A. Pfitzner, T. Doert, P. Böttcher, *Chem. Mater*. **2004**, *16*, 806.
[5] T. Nilges, C. Dreher, A. Hezinger, *Solid State Sci*. **2005**, *7*, 79.
[6] T. Nilges, S. Lange, *Z. Anorg. Allg. Chem*. **2005**, *631*, 3002.
[7] T. Nilges, S. Lange, *Z. Anorg. Allg. Chem*. **2004**, *630*, 1749.
[8] B. Reuter, K. Hardel, *Naturwissenschaften* **1961**, *48*, 161.
[9] B. Reuter, K. Hardel, *Z. Anorg. Allg. Chem*. **1965**, *340*, 168.
[10] S. Hull, D. A. Keen, N. J. G. Gardner, W. Hayes, *J. Phys.: Condens. Matter*. **2001**, *13*, 2295.
[11] R. B. Beeken, K. L. Menningen, *J. Appl. Phys*. **1989**, *66*, 5340.
[12] R. B. Beeken, T. J. Wright, T. Sakuma, *J. Appl. Phys*. **1999**, *85*, 7635.
[13] S. Lange, T. Nilges, *Chem. Mater*. **2006**, *18*, 2538.
[14] S. Lange, M. Bawohl, D. Wilmer, H.-W. Meyer, H.-D. Wiemhöfer, T. Nilges, *Chem. Mater*. **2007**, *19*, 1401.
[15] W. F. Kuhs, *Acta Crystallogr*. **1992**, *A48*, 80.
[16] B. M. T. Willis, *Acta Crystallogr*. **1969**, *A25*, 277.
[17] R. Bachmann, H. Schulz, *Acta Crystallogr*. **1984**, *A40*, 668.
[18] U. H. Zucker, H. Schulz, *Acta Crystallogr*. **1982**, *A38*, 563.
[19] U. H. Zucker, H. Schulz, *Acta Crystallogr*. **1982**, *A38*, 568.
[20] C. Wagner, *J. Chem. Phys*. **1953**, *21*, 1819.
[21] J. Janek, C. Korte, *Solid State Ionics* **1996**, *92*, 193.
[22] H. Rickert, C. Wagner, *Ber. Bunsenges. Phys. Chem*. **1963**, *67*, 621.
[23] X-RED and X-SHAPE (versions 1.31 and 2.07), Programs for Absorption Correction, Stoe & Cie GmbH, Darmstadt (Germany) **2005**.
[24] V. Petricek, M. Dusek, L. Palatinus, JANA2000, The Crystallographic Computing System, Institute of Physics, Praha (Czech Republic) **2000**.